Soft-ratchet modeling of end-point memory in the nonlinear resonant response of sedimentary rocks

Oleksiy O. Vakhnenko,[1] Vyacheslav O. Vakhnenko,[2] and Thomas J. Shankland[3]
[1]*Department of Nonlinear Physics of Condensed Matter, Bogolyubov Institute for Theoretical Physics, 14-B Metrologichna Street, Kyïv 03143, Ukraïna*
[2]*Department of Dynamics of Nonhomogeneous Media, Institute of Geophysics, 63-B Bohdan Khmel'nyts'kyy Street, Kyïv 01054, Ukraïna*
[3]*Earth and Environmental Sciences Division, Los Alamos National Laboratory, Los Alamos, New Mexico 87545, USA*
(Received 26 October 2004; revised manuscript received 27 January 2005; published 6 May 2005)

We developed and thoroughly examined a model of longitudinal vibrational resonance in bar-shaped sedimentary rocks; these materials exhibit memory that originates from an essential asymmetry in processes of rupture and recovery of intergrain and interlamina cohesive bonds. The theory relies on an appropriate isolation and an adequate formalization of two mutually dependent subsystems, namely, a subsystem of ruptured bonds and a subsystem of internal longitudinal displacements. The subsystem of ruptured bonds is shown to be of a soft-ratchet type, so that its response to an alternating internal stress is characterized by broken symmetry and appears as nonzero long-term temporal and spatial changes in the concentration of ruptured bonds. The internal stress is generated by an alternating external drive acting both directly through the subsystem of longitudinal displacements and indirectly through temporal and spatial modifications of Young's modulus due to changes in concentration of ruptured bonds. The scheme reproduces the main experimental effects by using the simplest linear form of attenuation in an elastic subsystem and realistic assumptions about the stress-strain relation. In particular, it correctly describes: hysteretic behavior of a resonance curve on both its upward and downward slopes; linear softening of resonant frequency with increase of driving level; gradual (almost logarithmic) recovery (increase) of resonant frequency at low dynamical strains after the sample was conditioned by high strains; and temporal relaxation of response acceleration amplitude at fixed frequency. These are the most interesting observations typical of forced longitudinal oscillations of sandstone bars in the nonlinear regime. Further, we are able to trace how water saturation enhances the hysteresis and simultaneously decreases the quality factor because of an increase in equilibrium concentration of ruptured cohesive bonds. We also predict theoretically a dynamical effect analogous to the widely known quasistatic effect of hysteresis with discrete (end-point) memory.

DOI: 10.1103/PhysRevB.71.174103 PACS number(s): 62.30.+d, 62.40.+i, 62.20.Mk, 83.80.Fg

I. INTRODUCTION

Sedimentary rocks, particularly sandstones, are distinguished by their grain structure[1–3] in which the core of each grain is much harder than the intergrain cementation material.[4] Imperfect intergrain cementation partially appears as porosity,[1–3] a property governing rock permeability that is essential, e.g., for petroleum production.[1,2] In addition, porosity facilitates penetration of water into areas of intergrain contacts[1,2] causing a dramatic impact on elastic moduli[5–7] and seismic dissipation factors.[5–8] The peculiarities of grain and pore structures give rise to a variety of remarkable nonlinear mechanical properties demonstrated by rocks, both at quasistatic and alternating dynamic loading. Thus, the hysteresis earlier established for the stress-strain relation in samples subjected to quasistatic loading-unloading cycles[9,10] has also been discovered for the relation between acceleration amplitude and driving frequency in bar-shaped samples subjected to an alternating external drive that is frequency-swept through resonance.[11–13] At strong drive levels there is an unusual, almost linear decrease of resonant frequency with strain amplitude,[12,14,15] and there are long-term relaxation phenomena[13,16] such as nearly logarithmic recovery (increase) of resonant frequency after the large conditioning drive has been removed.[15]

The fragmentary understanding of these observations[15,17] has stimulated us to look into the whole problem, usually characterized as "slow dynamics," more systematically and to propose a closed-form theory. This is based upon an explicit, physically motivated formalization of a sandstone bar system as two coupled nonlinear subsystems, one of which breaks the symmetry of system response to an alternating external drive and acts as a sort of soft ratchet or leaky diode.[18] We specify these subsystems as a fast subsystem of longitudinal displacements and a slow subsystem of ruptured intergrain and/or interlamina cohesive bonds.

In this paper we present a detailed development of a model,[18] and we inspect its ability to explain numerous experimental observations seen in forced longitudinal oscillations of sandstone bars. We demonstrate that a broad set of experimental data can be understood as various facets of the same internally consistent approach. Furthermore, the suggested theory will be shown to predict the dynamical realization of hysteresis with end-point memory, figuratively resembling its well-known quasistatic prototype[9,10] (see also more recent publications[4,11]).

II. SUBSYSTEM OF LONGITUDINAL DISPLACEMENTS

A reliable probing method widely applied in resonant bar experiments is to drive a horizontally suspended cylindrical sample with a piezoelectric force transducer cemented between one end of the sample and a massive backload, and to simultaneously measure the sample response with a lightweight accelerometer attached to the opposite end of the bar.[13,15] In this case the alternating strain configuration inside the bar is principally longitudinal, and has to be treated as kinematically excited.[19] The relevant boundary conditions for the field of longitudinal displacements u are as follows:

$$u(x=0|t) = D(t)\cos\left[\varphi + \int_0^t d\tau\omega(\tau)\right], \tag{1}$$

$$\sigma(x=L|t) + \gamma\frac{\partial^2 u}{\partial x\,\partial t}(x=L|t) = 0, \tag{2}$$

where t is time and x denotes the running longitudinal Lagrange coordinate of the bar with $x=0$ and $x=L$ marking its driven and free ends, respectively. As a rule, the driving amplitude $D(t)$ is set to be basically constant except for the moments when the driving device is switched on, is switched into another constant driving level, or is switched off, whereas the time dependence of cyclic driving frequency $\omega(t)$ is prescribed by the type of frequency sweep. Another kind of experiment where the parts played by the driving amplitude $D(t)$ and the driving frequency $\omega(t)$ are reversed would also be informative.

For the evolution equation for the field of longitudinal displacements (referred to also as the elastic subsystem) we write the most general form

$$\rho\frac{\partial^2 u}{\partial t^2} = \frac{\partial\sigma}{\partial x} + \frac{\partial}{\partial x}\left[\frac{\partial\mathcal{F}}{\partial(\partial^2 u/\partial x\partial t)}\right] \tag{3}$$

evaluating its content step-by-step. Thus, the dissipative function $\mathcal{F}$ must be some even function of strain velocity $\partial^2 u/\partial x\partial t$ in order to ensure both the positiveness and the internal character of dissipation. Here we restrict ourselves to the Stokes internal friction[20] associated with the dissipative function

$$\mathcal{F} = (\gamma/2)[\partial^2 u/\partial x\partial t]^2. \tag{4}$$

The quantities ρ and γ are, respectively, the mean density of sandstone and the coefficient of internal friction in an elastic subsystem. In what follows, the dependences of ρ and γ in Eqs. (3) and (4) on temperature T, water saturation s, and strain $\partial u/\partial x$ will be ignored. The stress-strain relation $(\sigma-\partial u/\partial x)$ we adopt in the form

$$\sigma = \frac{E\ \mathrm{sech}\ \eta}{(r-a)[\cosh\ \eta\,\partial u/\partial x + 1]^{a+1}} - \frac{E\ \mathrm{sech}\ \eta}{(r-a)[\cosh\ \eta\,\partial u/\partial x + 1]^{r+1}} \tag{5}$$

which at $r>a>0$ allows one to block the bar compressibility at strain $\partial u/\partial x$ tending toward $+0-\mathrm{sech}\ \eta$. Thus, the parameter $\cosh\ \eta$ is assigned for a typical distance between the centers of neighboring grains divided by the typical thickness of intergrain cementation contact, while the exponents r and a characterize the repulsive and the attractive parts of intergrain interaction, respectively. In other words, we approximate the potential of grain-grain interaction by the empirical Mie potential. At small strains $|\partial u/\partial x| \ll \mathrm{sech}\ \eta$ we obtain

$$\frac{\sigma}{E\partial u/\partial x} \approx 1 - \tfrac{1}{2}(r+a+3)\cosh\ \eta\,\partial u/\partial x + \tfrac{1}{6}(r^2+ra+a^2+6r+6a+11)(\cosh\ \eta\,\partial u/\partial x)^2 \tag{6}$$

and, hence, the parameters r, a, $\cosh\ \eta$ are seen to completely specify the nonlinear corrections to Hooke's law, provided that a direct influence of strain $\partial u/\partial x$ on Young's modulus E is absent. Meanwhile, the indirect effect of strain on Young's modulus, namely the impact mediated by the concentration c of ruptured intergrain cohesive bonds, will be incorporated in our theory as the main source of all nontrivial phenomena mentioned in the Introduction. We shall refer to this subject in the next section.

III. SUBSYSTEM OF RUPTURED COHESIVE BONDS

Any dynamical model dealing exclusively with a single subsystem of longitudinal displacements is incapable of reproducing the entire suite of phenomena exhibited by sandstones in resonant bar experiments without invoking speculative assumptions (e.g., temporal evolution of the amplitude-frequency characteristic[17]) that does not follow from the original equation or without incorporating auxiliary quantities (e.g., maximum strain excursion[17]) that can be justified only for the quasistatic theory. When holding this position one is unable to depart from an incomplete, fragmentary description. At best, one may have to appeal to a hypothetical slow subsystem only in a rather artificial way,[15,17] i.e., without explicit specification of all relevant (dynamic or kinetic) independent variables and their governing evolution equations, not to mention the mutual feedback between the slow subsystem and the fast elastic one.

We overcome the difficulties of single-subsystem modeling by introducing along with the fast elastic subsystem a slow subsystem of ruptured intergrain cohesive bonds via their concentration c. At any given stress σ (tensile or compressive) the quantity c must evolve to its stress-dependent equilibrium value c_σ. In order to achieve reliable consistency between theory and experiment such an evolution has to be treated as being nearly logarithmic rather than exponential on the one hand and as being sensitive to the sign of the applied stress on the other. Both of these aspects can be readily included in the concept of blended kinetics which is believed to find more or less natural physical justification in consolidated materials. The idea consists of presenting the actual concentration of defects c as some reasonable superposition of constituent concentrations g, where each particular g is proved to obey rather simple kinetics.

We start with considering a set of constituent concentrations. Every particular concentration g in this set is assumed

to evolve to its stress-dependent equilibrium value g_σ with the velocity $\partial g/\partial t$ that in lowest order approximation should be proportional to the difference $g_\sigma - g$. Thus, at $g > g_\sigma$ the ruptured bonds are becoming restored ($\partial g/\partial t < 0$) while at $g < g_\sigma$ the unruptured bonds are becoming broken ($\partial g/\partial t > 0$). Denoting the restoring rate as $\mu = \mu_0 \exp(-U/kT)$ and the rupturing rate as $\nu = \nu_0 \exp(-W/kT)$ we can formalize the earlier statements in terms of the following kinetic equation:

$$\partial g/\partial t = -[\mu\theta(g - g_\sigma) + \nu\theta(g_\sigma - g)](g - g_\sigma), \tag{7}$$

where U and W are the activation barriers for the processes of bond restoration and bond rupturation, respectively, k is the Boltzmann constant, and $\theta(z)$ designates the Heaviside step function.

There is a question whether the rates μ and ν should be the same or different and why. We argue that the parameters μ and ν have to differ substantially inasmuch as the volume attributed to generate a single crack turns out to be essentially mesoscopic although confined to an intergrain space.

Indeed, under a tensile load there are an immense number of spatial ways for a mesoscopic intergrain cementation contact to be broken with the same basic result: creation of an intergrain crack. Here we understand that any relevant macroscopic characteristic of rock is bound to be insensitive to the particular position of a crack between given neighboring grains but should essentially depend on the cumulative area of cracks per unit volume which can serve as an appropriate measure for the concentration of defects. Similarly, there are various ways for an already existing crack in equilibrium to be further expanded when surplus tensile load is applied. However, under compressive load a crack, once formed, has only one spatial way to be annihilated or contracted. These are the key observations that imply a large disparity $\nu_0 \gg \mu_0$ between the rates ν_0 and μ_0 regardless of the cohesive properties of the cementation material. Moreover, because of possible water intercalation and/or fine fragmentation of cementation material between opposite faces of a crack, we can expect the typical value of U to exceed that of W. In combination all these factors might sustain an even greater disparity $\nu \gg \mu$ between the actual rates ν and μ of defect creation and defect annihilation that may amount to many orders. This conclusion, which relies on the mesoscopic scale of the structural elements involved, finds a natural analogy on the macroscopic level when samples once having been broken remain broken practically forever.

Up to now we specified only a particular constituent concentration of defects g that can be labeled by the pair of fixed activation parameters U and W. In reality, any small but still macroscopic volume of sandstone contains a huge variety of structural elements distinguished by size, composition, natural cleavage, etc. As a result, activation barriers for the process of cohesion restoration U and the process of cohesion rupture W have to be distributed over some ranges, which we denote as $U_0 \leqslant U \leqslant U_0 + U_+$ and $W_0 \leqslant W \leqslant W_0 + W_+$, respectively. Although the types of these distributions are unknown, their characteristics U_0, U_+ and W_0, W_+ must be insensitive to a particular choice of bar's cross section in accordance with specimen homogeneity (similarity) on the macroscopic scale. Of course, the very number of these characteristics is insufficient to specify the set of constituent concentrations constructively, i.e., we still lack a definite recipe for how (with what weight) any constituent concentration of defects g should contribute to the actual (averaged) concentration of defects c. Thus, to proceed further some additional assumptions about the distributions of activation barriers must be added. For the sake of definiteness we approximate the barriers U and W as distributed independently and uniformly within the intervals given earlier. Thus, the relative number of restoration barriers in the interval dU surrounding U at W being fixed is taken to be $\theta(U - U_0)\theta(U_0 + U_+ - U)dU/U_+$, while the relative number of rupturation barriers in the interval dW surrounding W at U being fixed is taken to be $\theta(W - W_0)\theta(W_0 + W_+ - W)dW/W_+$. As a consequence the actual concentration of ruptured cohesive bonds c is determined by the constituent concentration g via the formula

$$c = \frac{1}{U_+ W_+} \int_{U_0}^{U_0 + U_+} dU \int_{W_0}^{W_0 + W_+} dW \cdot g. \tag{8}$$

This expression does not contradict the next assumption

$$g_\sigma = c_\sigma \tag{9}$$

relating the equilibrium value of actual concentration of ruptured bonds c_σ to the equilibrium value of constituent concentration of ruptured bonds g_σ, where both c_σ and g_σ are prescribed by the stress σ. As a matter of fact, only the quantity c_σ might find a legitimate place in standard thermodynamical estimations,[21–23] whereas in dealing with g_σ we must lean upon more or less plausible conjecture, e.g. as established by formula (9).

According to Kosevich[21,22] the equilibrium concentration of defects associated with a stress σ is given by the expression

$$c_\sigma = c_0 \exp(v\sigma/kT), \tag{10}$$

where the parameter $v > 0$ stands for a typical volume accounting for a single defect and characterizes the intensity of dilatation. Although formula (10) should supposedly be applicable to the ensemble of microscopic defects in crystals, it was derived in the framework of continuum thermodynamic theory that does not actually need any specification of either the typical size of elementary defect or the particular structure of the crystalline matrix. For this reason we believe it should also work for an ensemble of mesoscopic defects in consolidated materials, provided that for a single defect we shall understand some elementary rupture of intergrain cohesion. The equilibrium concentration of defects in an unstrained, completely recovered bar c_0 has to be some function of temperature T and water saturation s. The particular character of these dependences does not follow from first principles and needs to be extracted from experiments.

At this point we introduce a phenomenological relationship between defect concentration c and Young's modulus E. Intuition suggests that E must be some monotonically decreasing function of c, which can be expanded in a power series with respect to a small deviation of c from its unstrained equilibrium value c_0. In the lowest approximation

we can drop all powers except the zeroth and first and as a result safely rearrange the required relation into the form

$$E = (1 - c/c_{\mathrm{cr}})E_{+}. \tag{11}$$

Here c_{cr} and E_{+} are the critical concentration of defects and the maximum possible value of Young's modulus, respectively. Both of these parameters we take to be independent of temperature and water saturation.

According to relationship (11) the actual concentration of defects c is incorporated into the evolution equation for the elastic subsystem (3) as normalized by its critical value c_{cr}. For this reason there is no need to supply the quantities c, c_{σ}, and c_{cr} by any particular units, though the units must be the same for all three quantities. As for the units of the running and equilibrium constituent concentrations g and g_{σ} it is sufficient to know only their relationship to the units of actual concentration given by expression (9).

At constant load the kinetic Eq. (7) ensures that the concentration c tends to its equilibrium value c_{σ} given by formula (10) and as a consequence Young's modulus (11) attains the magnitude

$$E_{\sigma} = [1 - (c_0/c_{\mathrm{cr}})\exp(v\sigma/kT)]E_{+}. \tag{12}$$

It is worth noticing that the resulting functional dependence of E_{σ} on σ almost exactly matches the experimentally established fitting formula for elastic moduli as a function of an applied load $P \sim -\sigma > 0$ (see, e.g., Ref. 24, and references therein). Furthermore, relation (12) taken at zero stress $\sigma = 0$ allows us to reconstruct the temperature and saturation dependences of the unstrained equilibrium concentration of defects c_0 using available experimental data for Young's modulus E_0 in unstrained, recovered samples. Thus, if we take into account the Sutherland temperature extrapolation[25,26] and analyze temperature-dependent data at zero saturation[27] plus saturation-dependent data at room temperature[7] (selected for Berea sandstone), we are able to suggest the following fitting formula:

$$c_0 = c_{\mathrm{cr}}\left(\frac{T}{T_{\mathrm{cr}}}\right)^2\left[\cosh^2\alpha - \exp\left(-\frac{\beta s}{1-s}\right)\sinh^2\alpha\right], \tag{13}$$

where saturation s varies within the interval $0 \leqslant s \leqslant 1$. The fitting parameters relevant for Berea sandstone are as follows $T_{\mathrm{cr}} = 1475$ K, $\cosh^2\alpha = 16$, $\beta = 10$. At $s \neq 0$ our approximation is expected to work at least within the temperature range between irreversible damage thresholds of sedimentary rocks, namely between the freezing-point of pore water ($\approx$273 K) and the baking point of interstitial clays ($\approx$345 K).

The significant issue of our approach is contained in the kinetic Eq. (7) that can be applied to both static and dynamic regimes of external load. In the latter case, however, for c_{σ} and g_{σ} we must consider the would-be equilibrium quantities, i.e., quantities given by formulas (10) and (9) where the stress σ is taken to be dynamical.

At small dynamical stresses $|\sigma| \ll kT/v$ the exponent $\exp(v\sigma/kT)$ dominating the expression (10) for c_{σ} can be readily approximated by the two first terms in its expansion. Because of relation (9) a similar approximation applies for g_{σ}. Nevertheless, this fact does not indicate a zero-valued, long-term correction to g_0 in the solution g of the kinetic Eq. (7) as might be roughly expected. On the contrary, the great disparity $\nu \gg \mu$ between the rate of defect creation ν and the rate of defect annihilation μ turns out to provide the physical mechanism that breaks the symmetry of system response to an alternating external drive and acts as a sort of soft ratchet or leaky diode. It is the core of this modeling.

In contrast, earlier theories of inelastic relaxation developed for crystalline solids[23] rely upon a symmetric form of the kinetic equations (corresponding to $\mu \equiv \nu$ in our notations) and do not assume the equilibrium value of the internal relaxation parameter (corresponding to g_{σ} in our notations) to be driven dynamically. Also, earlier theories of crack formation[28] differ from our approach in that they neglect the possibility of crack recuperation (i.e., they assume $\mu = 0$ in our notations) and do not incorporate a variable concentration of defects into the right-hand side of the appropriate kinetic equation.

Summarizing the content of the second and third sections, we have formulated the principal theoretical propositions of our model and have formalized them in terms of two coupled, essentially nonlinear subsystems. First, we have suggested a dynamical equation for the field of longitudinal displacements (3) with the appropriate specification of the dissipative function (4), the stress-strain relation (5), and the impact of defect concentration on Young's modulus (11). Second, we have developed a soft-ratchet-type kinetic equation for the constituent concentration of defects (ruptured intergrain cohesive bonds) (7) with the appropriate specifications of stress-guided, would-be equilibrium constituent concentration of defects (9) and would-be equilibrium actual concentration of defects (10) and have adopted a reasonable relation between the constituent concentration and the actual concentration of ruptured intergrain cohesive bonds (8). We also have presented boundary conditions for the field of longitudinal displacements (1) and (2) allowing us to formalize the effect of the transducer on the whole bar system.

The only thing remaining to be specified is the initial conditions. These must depend on the sample's prehistory. Thus, for the unstrained, completely recovered bar the initial conditions are written as follows:

$$u(x|t=0) = 0, \quad \frac{\partial u}{\partial t}(x|t=0) = 0, \tag{14}$$

$$g(x|t=0) = c_0, \tag{15}$$

where $0 < x < L$.

IV. SOFT-RATCHET KINETICS UNDER AN ALTERNATING DRIVE

In this section we illustrate two different kinetic regimes of defect creation and annihilation under an alternating drive that can be the basic to qualitative understanding of experimental results as well as their computerized replicas. For this purpose we introduce a quantity (the surplus constituent concentration)

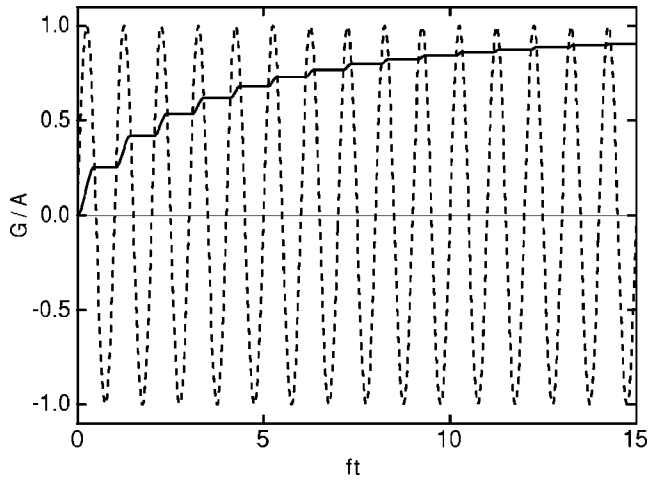

FIG. 1. Normalized solution G/A of the soft-ratchet kinetic Eq. (18) with sinusoidal stimulation (17) at $\mu=1\ \mathrm{s}^{-1}$, $\nu=4000\ \mathrm{s}^{-1}$, $f\equiv\omega/2\pi=4000$ Hz, $\delta=0$, and the initial condition $G(t=0)=0$ (solid steplike line). The dashed line indicates the normalized sinusoidal stimulation $G_\sigma/A=\sin\omega t$. Time along the abscissa is normalized to the oscillation period $1/f$.

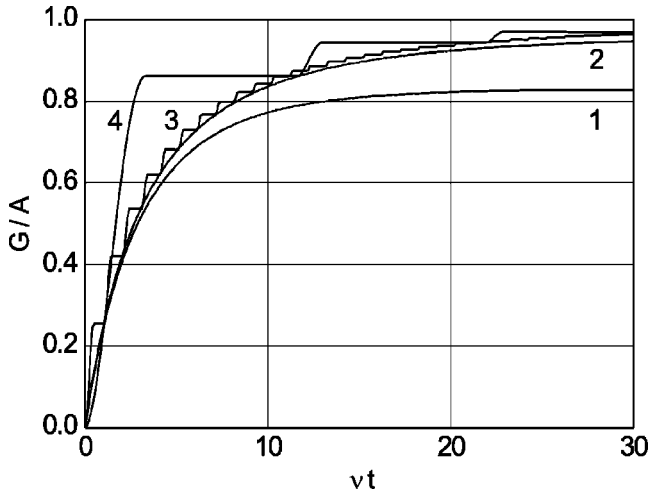

FIG. 2. Normalized solution G/A of the soft-ratchet kinetic Eq. (18) under sinusoidal stimulation (17). Curves $j=1,2,3,4$ correspond to successively higher rates of defect creation $\nu_j=4\cdot 10^j\ \mathrm{s}^{-1}$ with all other parameters from Fig. 1 being preserved. Time on the abscissa is normalized to the inverse rate of defect creation $1/\nu$ separately for each curve.

$$G\equiv g-g_0 \tag{16}$$

that measures the excess $G>0$ or shortage $G<0$ of defects relative to the unstrained background g_0, and we approximate the impact of the dynamic subsystem onto the kinetic subsystem by a single harmonic

$$G_\sigma\equiv g_\sigma-g_0=A\sin(\omega t+\delta), \tag{17}$$

where A and δ are some functions of the longitudinal coordinate x. Their particular forms do not need to be specified because at each fixed x the quantity G obeys the ordinary differential equation

$$dG/dt=-[\mu\theta(G-G_\sigma)+\nu\theta(G_\sigma-G)](G-G_\sigma). \tag{18}$$

Note, however, that to lowest order the amplitude A is proportional to the amplitude ε of strain

$$\partial u/\partial x=\varepsilon\sin(\omega t+\delta) \tag{19}$$

taken in the same single mode approximation. The proportionality coefficient vc_0E/kT can be readily extracted from expressions (17) and (19) by using the approximate stress-strain relation $\sigma=E\partial u/\partial x$ and formulas (9) and (10) for g_σ and c_σ. Here for simplicity we ignore the time dependence of Young's modulus through the total concentration of defects.

Starting from the zeroth value $G(t=0)=0$ the kinetic Eq. (18) and the sinusoidal drive (17) cause surplus constituent concentration G to grow in each cycle in a nearly steplike fashion for $\mu\ll\nu\lesssim\omega/2\pi$ (Fig. 1). Time intervals of fast increase controlled by rate ν are determined from the inequality

$$A\sin(\omega t+\delta)-G(t)>0 \tag{20}$$

whereas time intervals of slow decrease controlled by rate μ are determined from the opposite inequality

$$A\sin(\omega t+\delta)-G(t)<0. \tag{21}$$

A time interval of increase is followed by a time interval of decrease and vice versa yielding a net full step in each cycle $2\pi/\omega$.

Although the kinetic Eq. (18) could be integrated analytically at every time interval where either inequality (20) or (21) holds, it is impractical to match such piecewise solutions into concise expression suitable for qualitative analysis. Instead, even a quick look at the computer solutions (Fig. 2) is sufficient to evaluate the mean (time-averaged) magnitude H of the steady-state solution for G in comparison with the amplitude A as well as to estimate the effective rate λ of cyclic buildup of surplus constituent concentration G under an oscillating load in comparison with the rate ν of monotonic growth of G under a constant tensile load. In preparing Fig. 2 we took the rate μ to coincide with its maximum value $\mu_0\exp(-U_0/kT)=1\ \mathrm{s}^{-1}$, which in Sec. V will be adopted for interpreting experimental results on slow dynamics. The frequency $f\equiv\omega/2\pi$ was chosen to be 4000 Hz, and the rate ν was tested at four essentially different values 40, 400, 4000, and 40 000 s^{-1} (Fig. 2, curves 1, 2, 3, and 4, respectively). All four curves strongly indicate that for $\nu\geqslant 0.01f$ the effective rate λ of cyclic buildup does not drop more than five or six times below the rate ν. Moreover, at $\nu\geqslant 0.01f$ the ratio H/A always exceeds value of 0.8 and rapidly approaches unity as the ratio ν/f increases. Another significant observation consists of the almost total suppression of periodical fluctuations of steady-state solution G around its mean value H (Fig. 3).

The results of the previous paragraph can be readily applied to the case when the amplitude A is not constant but grows with time sufficiently slowly such that $0<\dot{\varepsilon}/\varepsilon\ll\lambda\sim 0.2\nu$; the overdot denotes the derivative with respect to time t. Then at $\nu\gtrsim 0.01f$ we can safely treat the surplus

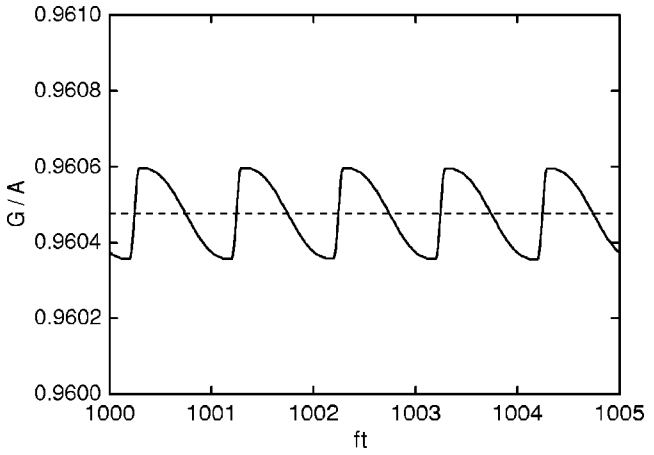

FIG. 3. Normalized solution G/A of the soft-ratchet kinetic Eq. (18) at an essentially steady stage of its evolution (solid line). The dashed line represents the mean value H/A of the normalized steady-state solution. Conditions used for calculations of curve 2 from Fig. 2 are preserved. Time along the abscissa is normalized to the oscillation period $1/f$.

defect concentration G as a time dependent quantity that effectively tracks amplitude A. There is every reason to believe that both the above requirements are fulfilled in resonant bar experiments as frequency sweeps toward a resonance. Thus, the inequality $0<\dot{\varepsilon}/\varepsilon \ll 0.2\nu$ is maintained by the fact that typical sweeps around resonance[13] are unable to sustain the rate $|\dot{\varepsilon}|/\varepsilon$ by more than 0.5 s^{-1}. As for the inequality $0.01f \lesssim \nu$, it seems to be in line with our hypothesis of strong inequality $\mu \ll \nu$ secured by many orders as given in Sec. III.

We now inspect the regime of slow relaxation in the subsystem of intergrain ruptured bonds. This regime occurs after the surplus constituent concentration G has been pumped to some steady-state magnitude B and then the conditioning oscillating drive is drastically reduced at time $t=t_c$. In this case, i.e., at $t>t_c$, the strong inequality $B \gg A$ holds, and the elastic subsystem serves only for probing the resonant frequency, while its impact on the subsystem of ruptured bonds can be totally neglected. Thus, we omit the term G_σ throughout the kinetic Eq. (18) and obtain

$$dG/dt = -\mu G \tag{22}$$

bearing in mind that the regime of interest starts at $t=t_c$ with $G(t=t_c)=B$. Here the quantity B is estimated to be

$$B = c_0\left[\exp\left(\frac{v\sigma_+}{kT}\right) - 1\right] \tag{23}$$

where $\sigma_+>0$ stands for the maximum stress determined by the amplitude of stress oscillations under dynamical conditioning.

The approach just formulated is undoubtedly valid to describe the process of relaxation after tensile static conditioning when σ_+ should be understood as the positive end-point stress. We expect it also could be applied to treat relaxation phenomena after an abrupt thermal disturbance provided σ_+ is identified with some effective rupturating stress predetermined by the absolute value of thermal shock.

The kinetic Eq. (22) for surplus constituent concentration G yields an exponential decay

$$G = B\exp[-\mu(t-t_c)] \tag{24}$$

at $t \geqslant t_c$. However, this by no means causes the actual surplus of defect concentration $c-c_0$ to diminish exponentially. On the contrary, inserting the solution (24) into the formula (8) with the use of definition (16) we easily obtain

$$c = c_0 + \frac{B}{\chi}\{E_1[\tau\exp(-\chi)] - E_1(\tau)\}. \tag{25}$$

Here

$$\tau \equiv \mu_0\exp(-U_0/kT)(t-t_c) \tag{26}$$

denotes a unitless time, whereas

$$\chi \equiv U_+/kT \tag{27}$$

determines a unitless width of energy interval occupied by the distribution of activation barriers for the process of cohesion restoration. Finally

$$E_1(z) = \int_1^\infty \frac{dy}{y}\exp(-zy) \tag{28}$$

designates the integral exponential function.[29]

Despite its name, $E_1(z)$ initially behaves logarithmically as clearly seen in its analytic expansion for $z<1$[29]

$$E_1(z) = -C - \ln z - \sum_{n=1}^{\infty}(-1)^n\frac{z^n}{n\cdot n!} \tag{29}$$

where $C \simeq 0.577\,215\,7$ stands for the Euler-Mascheroni constant. In its final stages $z>1$, however, use of the asymptotic series[29]

$$E_1(z) = \frac{\exp(-z)}{z}\left[1 + \sum_{n=1}^{\infty}(-1)^n\frac{n!}{z^n}\right] \tag{30}$$

turns out to be appropriate.

We apply expansions (29) and (30) to the most plausible case of $\exp(\chi) \gg 1$ and approximate the difference $E_1[\tau\exp(-\chi)]-E_1(\tau)$ controlling the temporal restoration of defect concentration (25) by the following piecewise formula:

$$E_1[\tau\exp(-\chi)] - E_1(\tau) \simeq \begin{cases} \chi - \tau + \tau^2/4 + \tau\exp(-\chi) & \text{at } \tau < \xi_- \\ \chi - C - \ln\tau + \tau\exp(-\chi) & \text{at } \xi_- \leqslant \tau \leqslant \xi_+ e^{\chi} \\ \dfrac{\exp[-\tau\exp(-\chi)]}{\tau\exp(-\chi)} & \text{at } \xi_+ e^{\chi} < \tau. \end{cases} \tag{31}$$

Here the constants $\xi_- \simeq 1.391\,099\,0$ and $\xi_+ \simeq 0.928\,630\,6$ are determined as the solutions of transcendental equations

$$-\xi_- + \xi_-^2/4 = -C - \ln\xi_- \tag{32}$$

and

$$-C-\ln\xi_+ + \xi_+ = \frac{\exp(-\xi_+)}{\xi_+}, \tag{33}$$

respectively. Equations (32) and (33) supply matching conditions to ensure that the piecewise representation (31) will be a continuous function at points $\tau=\xi_-$ and $\tau=\xi_+\exp(\chi)$, respectively. The larger the inequality $\exp(\chi)\gg 1$, the longer becomes the interval of almost logarithmic time dependence in formula (31).

Formulas (23), (25), and (31) substituted into the linear relationship (11) between Young's modulus E and the concentration of defects c allow us to analytically reproduce the slow, nearly logarithmic recovery (increase) of Young's modulus

$$E = \left(1-\frac{c_0}{c_{\rm cr}}\right)E_+ - E_+\frac{c_0}{c_{\rm cr}}\left[\exp\left(\frac{v\sigma_+}{kT}\right)-1\right] \times\left\{1-C\frac{kT}{U_+}-\frac{kT}{U_+}\ln\left[\mu_0\exp\left(-\frac{U_0}{kT}\right)(t-t_c)\right] + \frac{kT}{U_+}\mu_0\exp\left(-\frac{U_0+U_+}{kT}\right)(t-t_c)\right\} \tag{34}$$

over the very wide time interval

$$\frac{\xi_-}{\mu_0}\exp\left(\frac{U_0}{kT}\right) < t-t_c < \frac{\xi_+}{\mu_0}\exp\left(\frac{U_0+U_+}{kT}\right). \tag{35}$$

This type of recovery is experimentally observed by monitoring temporal variation of resonant frequency after the conditioning drive has been removed.[15]

The idea supporting the logarithmic recovery of Young's modulus had earlier been advocated by Ten Cate, Smith and Guyer,[15] although without identifying the proper time interval (35) where the logarithmic dependence holds and omitting the small linear correction [the last term in parentheses of expression (34)] to the leading logarithmic pattern. It is interesting to note that logarithmic kinetics also have been attributed to the process of moisture-induced aging in granular media.[30]

V. FORCED LONGITUDINAL OSCILLATIONS OF SANDSTONE BARS: COMPUTERIZED REPLICAS OF ACTUAL EXPERIMENTS

The vast majority of experimental results on forced longitudinal oscillations of sandstone bars use slow, stepwise frequency sweeps over one of the bar resonant frequencies.[11–15] A rough estimation based on the linear theory of kinematic excitation yields the fundamental frequencies

$$f_0(l) = \frac{2l-1}{4L}\sqrt{E_0/\rho} \quad (l=1,2,3,\ldots), \tag{36}$$

where E_0 is the Young's modulus in an unstrained, recovered sample given by formula (12) at $\sigma=0$, and attenuation γ is taken to be negligible. The relative positions of fundamental frequencies at finite attenuation as calculated for slow upward frequency sweep are displayed in Fig. 4. Here the resonance curve show the dependence of response amplitude R (taken on free end of the bar $x=L$) on drive frequency $f=\omega/2\pi$ at very small drive amplitude $D=7.6\cdot 10^{-9}\,L$ and with the model parameters as assumed for the next figure.

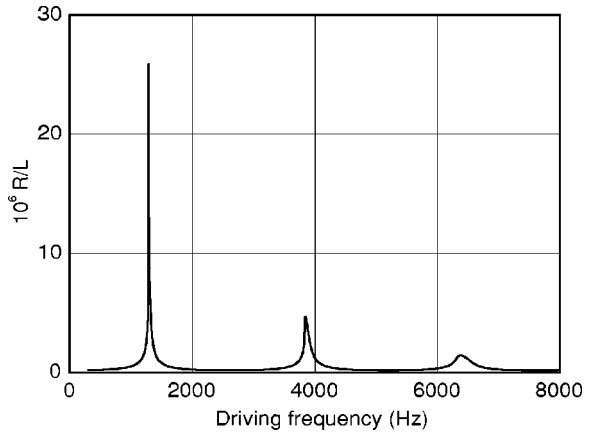

FIG. 4. Calculated resonance curve illustrating the relative positions of the first three resonance peaks under longitudinal kinematic excitation for a rock bar.

Figure 5 shows typical hysteretic resonance curves calculated in the vicinity of the second resonant frequency at successively higher drive amplitudes D. In order to achieve repeatable hysteresis each successive pair of curves was calculated following two preliminary sweep calculations. Such curves are usually referred to as being conditioned.[13] Arrows on the two highest curves indicate sweep directions. The cycle time for an up plus down sweep over the frequency interval 3700–4100 Hz was chosen to be 120 s. Model parameters were adopted to fit the experimental conditions and the experimental data as observed by Ten Cate and Shankland in experiments on Berea sandstone.[13] In particular, the ratio $E_+/\rho=7.439\cdot 10^6\ \mathrm{m}^2/\mathrm{s}^2$ was estimated from relationships (36), (12), and (13) with the second order frequency, bar length, temperature, and saturation as follows $f_0=3920$ Hz, $L=0.3$ m, $T=297$ K, and $s=0.25$. The ratio

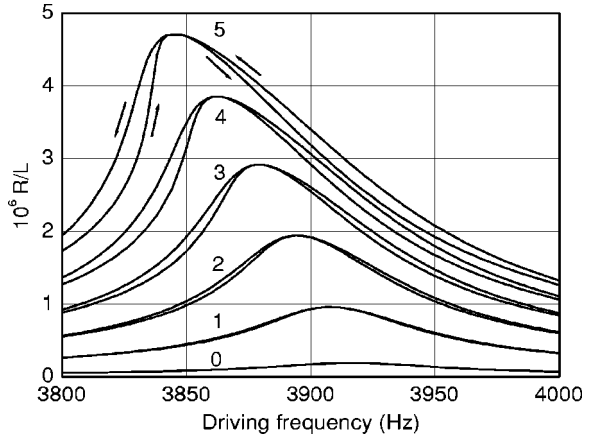

FIG. 5. Conditioned resonance curves $j=0,1,2,3,4,5$ at successively higher driving amplitudes $D_j=3.8(j+0.2\delta_{j0})10^{-8}\,L$. Arrows on the two highest curves indicate sweep directions. The absolute value of sweep rate is $|df/dt|=400$ Hz/min. Water saturation is taken to be $s=0.25$.

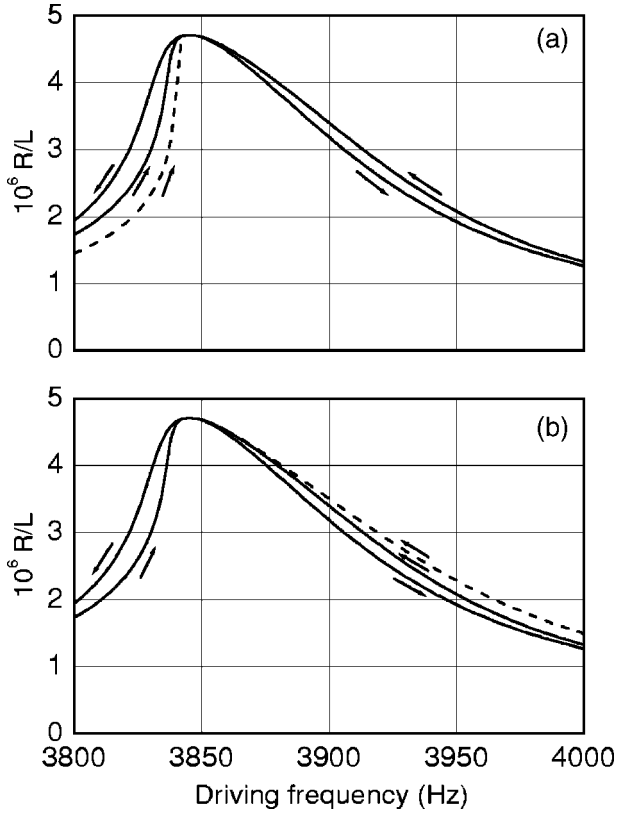

FIG. 6. Resonance curves at driving amplitude $D=1.9\cdot10^{-7}$ L. Arrows indicate sweep directions. The absolute value of sweep rate is $|df/dt|=400$ Hz/min. The dashed line in Fig. 6(a) represents the unconditioned initial curve made on the upward sweep. The dashed line in Fig. 6(b) represents the unconditioned initial curve made on the downward sweep.

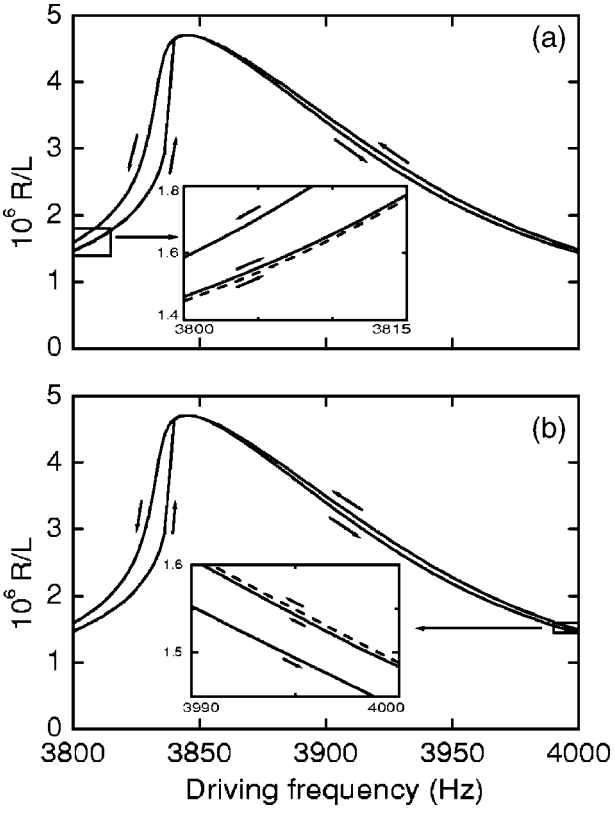

FIG. 7. Resonance curves at driving amplitude $D=1.9\cdot10^{-7}$ L. The absolute value of sweep rate is slowed to $|df/dt|=4$ Hz/min. Arrows indicate sweep directions. The dashed line in Fig. 7(a) resolvable only in the magnified inset represents the unconditioned initial curve made on the upward sweep. The dashed line on Fig. 7(b) resolvable in the magnified inset represents the unconditioned initial curve made on the downward sweep.

$\gamma/\rho=1.851$ m^2/s characterizing internal friction was chosen from the best fit of low amplitude theoretical curve (Fig. 5) to its experimental prototype[13] via comparison of quality factors. The parameters $\mu_0\exp(U_0/kT)=1$ s^{-1} and $U_+/k=2525$ K determining the character of slow relaxation were estimated in accordance with experimental measurements of temporal relaxation of response acceleration amplitude at fixed frequency[13] and observations of recovering resonant frequency as a function of time.[15] Due to the rather slow typical regimes of frequency sweep corresponding to actual experiments there is neither the experimental possibility nor the theoretical need to designate particular values for parameters $\nu_0\exp(-W_0/kT)$ and W_+/k that are responsible for defect creation kinetics. This is because above some critical value depending on driving frequency the combination $\nu_0\exp[-(W_0+W_+)/kT]$ gives rise to results indistinguishable from those obtained assuming the combination to be infinite. According to the estimations of previous section the condition that the kinetics of defect creation could be treated as practically instantaneous (i.e., formally characterized by infinite rate ν) is fulfilled already provided the inequality $0.01f_0\lesssim\nu_0\exp[-(W_0+W_+)/kT]$ holds. The combination of parameters $vE_+/k\cosh\eta=275$ K was chosen to quantitatively reproduce hysteretic phenomena in the sweep regimes typical of actual experiments.[13] Finally, the nonlinearity parameters $\cosh\eta=2300$, $r=4$, $a=2$ were estimated to map the true asymmetry of experimental resonance curves.[13]

From Fig. 5 we clearly see that at each level of external drive the effective width of resonance peak depends on the direction of frequency sweep being narrower for upward sweep (i.e., from lower to higher frequencies) than for downward sweep (i.e., from the higher to lower frequencies). As a result we observe the hysteretic loops formed by upward and downward curves both on their low and high-frequency slopes. Historically this effect proved to be the first manifestation of slow dynamics[13] caused according to our theory by the net creation of intergrain defects when the driving frequency closely approaches to resonance (i.e., when the amplitude of alternating stress increases) and rather slow their annihilation when the driving frequency departs from resonance (i.e., when the amplitude of alternating stress decreases). It is worth noticing that in the case of conditioned curves considered above annihilation of intergrain defects persists even when the driving frequency approaches resonance from far away until the amplitude of alternating stress overcomes some threshold above which defect creation prevails.

Figures 6(a) and 6(b) were calculated without any preliminary conditioning but with all model parameters for Fig. 5 preserved. The drive amplitude was chosen to be the same

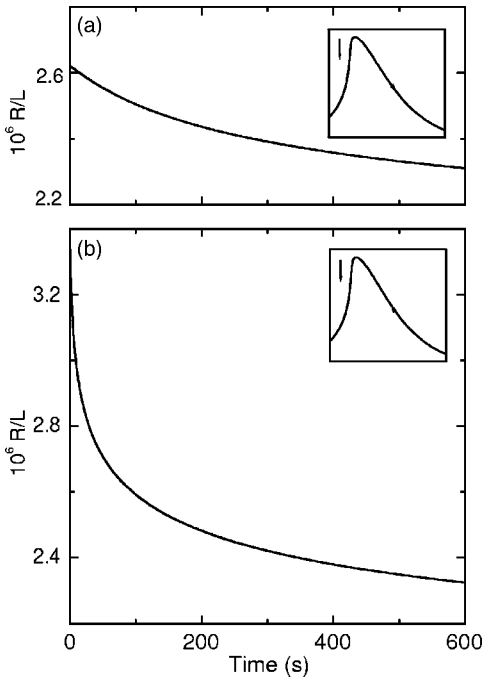

FIG. 8. Decay of response amplitude R at driving amplitude $D=1.9\cdot10^{-7}$ L and fixed frequency $f_s=3825$ Hz, lower than the peak frequency at $f_r=3846$ Hz. In Fig. 8(a) the sweep was stopped while making a repeatable upward sweep. In Fig. 8(b) the sweep was stopped while making a repeatable downward sweep.

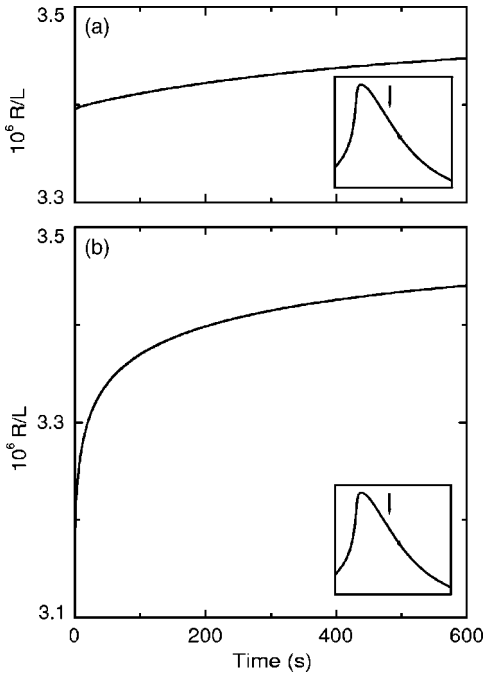

FIG. 9. Growth of response amplitude R at driving amplitude $D=1.9\cdot10^{-7}$ L and fixed frequency $f_s=3900$ Hz, higher than the peak frequency at $f_r=3846$ Hz. In Fig. 9(a) the sweep was stopped while making a repeatable downward sweep. In Fig. 9(b) the sweep was stopped while making a repeatable upward sweep.

as for two highest curves on Fig. 5. Thus Fig. 6(a) demonstrates three resonance curves obtained during the three successive (upward-downward-upward) frequency sweeps beginning with an upward sweep. The initial, unconditioned, curve marked by the dashed line lies below the two subsequent curves. Figure 6(b) demonstrates three resonance curves obtained during the three successive (downward-upward-downward) frequency sweeps beginning with a downward sweep. The initial curve marked by the dashed line lies above two subsequent curves. The curves marked by the solid lines in Figs. 6(a) and 6(b) are practically repeatable and coincide with the respective two highest curves on Fig. 5. All these results are in complete agreement with experimental observations.[13] The reason why the conditioned curve does not coincide with its unconditioned (initial) counterpart in the sweep interval between the starting frequency and the resonant frequency lies in the softer value of conditioned Young's modulus caused by an unrelaxed excess of defects created during the initial sweep.

As sweep rate decreases, the differences above become less pronounced thanks to the additional time for relaxation at each spanning frequency. This point is illustrated in Figs. 7(a) and 7(b) where the sweep rate was a hundred times slower than for Figs. 6(a) and 6(b). Nevertheless, even in this supposedly nonhysteretic case the memory of the highest strain amplitude still persists. The latter result characterized after its experimental detection[13] as "perhaps surprising" can be readily explained by the long-term recovery of Young's modulus dictated by the slow, almost logarithmic kinetics of defect annihilation [see formulas (34), (35), (25), and (31) from Sec. IV]. With still slower sweep times exceeding one day all three curves become indistinguishable regardless of direction of initial sweep. This theoretical result corroborates an indirect experimental indication in fixed-frequency measurements of acceleration that a sweep time of a few days in carefully controlled conditions would produce the same up and down resonance curves.[13]

Apart from the reason mentioned earlier, measurements of temporal relaxation of acceleration amplitude at fixed frequency provide experimental documentation of how a rock gradually loses memory of the highest strain,[13] and they thus elucidate the most interesting aspects of bond restoration kinetics. Figures 8 and 9 show theoretical relaxation curves that correctly reproduce the main features of the experiments.[13] While making a repeatable up or down resonance curve (with all model parameters the same as for the two highest curves of Fig. 5) we stopped the sweep at time t_s (drive still on) and calculated the amplitude of response R as a function of time $t-t_s$. As in the experiments the simulated response amplitude gradually decreased when the stopping frequency was lower than the resonant frequency [Figs. 8(a) and 8(b)] and increased when the stopping frequency was higher [see Figs. 9(a) and 9(b)]. Moreover, after approximately 10 min of relaxation the relaxation curves at a particular stopping frequency approached a long term level corresponding to the unconditioned part of the initial resonance curve whether or not the upward or downward preceding sweep was selected.

To reproduce another experimental facet of recovery time[13] we varied the previous simulations by stopping the sweep and simultaneously turning off the drive for 30 s with the sweep moving downward [Fig. 10(a)] or upward [Fig.

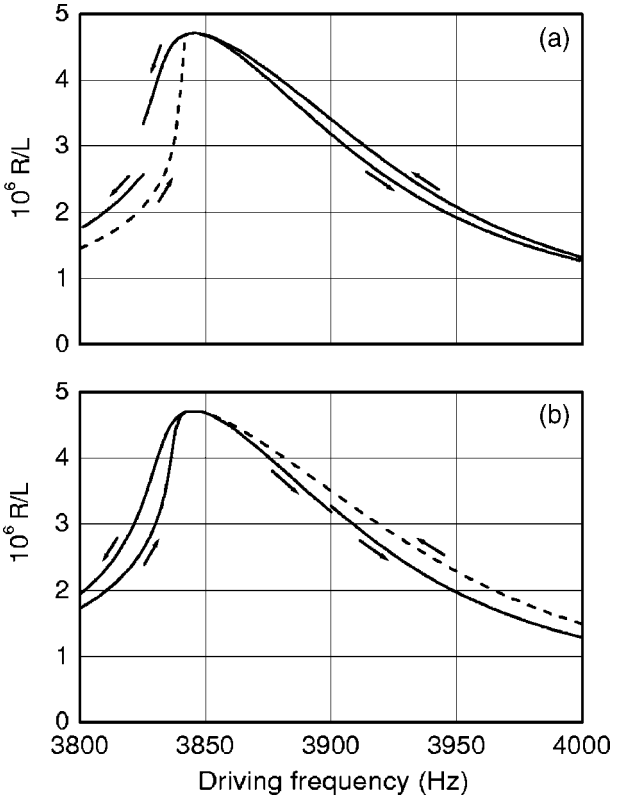

FIG. 10. (a) Resonance curves obtained by a continuous upward sweep and subsequent sectionally continuous downward sweep. During the downward sweep both drive and sweep were turned off simultaneously for 30 s at fixed frequency $f_s=3825$ Hz, lower than the peak frequency at $f_r=3846$ Hz. (b) Resonance curves obtained by continuous downward sweep and subsequent sectionally continuous upward sweep. During the upward sweep drive and sweep were turned off simultaneously for 30 s at fixed frequency $f_s=3900$ Hz, higher than the peak frequency at $f_r=3846$ Hz. For both pictures the driving amplitude and the absolute value of sweep rate when being turned on were $D=1.9\cdot10^{-7}$ and $|df/dt|=400$ Hz/min, respectively.

10(b)] from an already conditioned resonance. In a relatively short time (tens of seconds) the memory of the high strain amplitude rock had experienced at resonance diminished far more quickly than when the drive was left on. According to the kinetic Eq. (7) this distinction finds its rational explanation in a more favorable regime for defect annihilation under zero stress $\sigma=0$ in comparison with the regime governed by the oscillating stress of a considerable amplitude (though lesser than that at resonance). Figures 10(a) and 10(b) were prepared using the same model parameters as for Fig. 5. Also, drive amplitude and sweep rate (except the short time interval of drive and sweep stopping) were set to the same values as for the two highest curves in Fig. 5. Figure 10(a) displays the resonance curves obtained by the continuous sweep in upward followed by a sectionally continuous sweep downward. Figure 10(b) shows the complementary curves obtained by a continuous sweep downward followed by a sectionally continuous sweep upward. Effects of quick recovery (increase) of bar modulus E while sweep and drive were stopped are clearly seen as discontinuities in the curves.

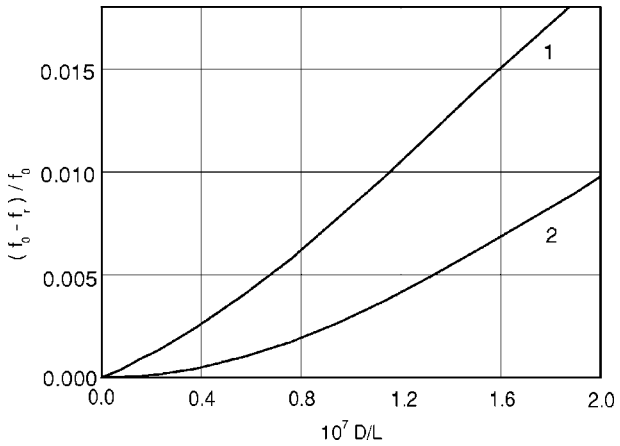

FIG. 11. Negative of the shift f_r-f_0 of peak frequency f_r from its asymptotic value f_0 as a function of normalized driving amplitude D/L for a hysteretic nonlinear material (curve 1) and for a classical nonlinear material with $v=0$ (curve 2).

At stopping frequencies below resonance response amplitude drops closer to the first (recovered) upward-swept curve marked on Fig. 10(a) by the dashed line. At stopping frequencies above resonance response amplitude jumps closer to the first (recovered) downward-swept curve marked in Fig. 10(b) by the dashed line. A qualitative view of these jumps comes from the indirect impact of strain on bar modulus through the concentration of defects. During the period of time when the sweep is approaching and passing resonance strain intensity becomes substantial causing a corresponding generation of defects, and the modulus decreases. This effect is manifested as a shift of resonance curve downward in frequency when the sweep has already passed resonance. If the drive and sweep are then turned off, the strain vanishes causing progressive annihilation of defects so that modulus increases. As a consequence the part of resonance curve, tracked after drive and sweep have been resumed, moves back (i.e., upward in frequency) as memory of the high strain is lost.

Figure 11 compares the shifts of resonant frequency as functions of driving amplitude at two different values of dilatation parameter v while other parameters were kept the same as in Fig. 5. Thus curve 1 calculated at $vE_+/k\cosh\eta=275$ K, for which strain-induced feedback between the slow and fast subsystems is substantial, demonstrates the almost linear dependence typical of materials with nonclassical nonlinear response, i.e., materials that possess the basic features of slow dynamics. In contrast, curve 2 calculated at $v=0$, when strain-induced excitation of the slow subsystem is absent and, hence, the mutual feedback between the slow and the fast subsystems is totally broken, demonstrates the almost quadratic dependence typical of materials with classical nonlinear response.[31] Closer inspection indicates that curve 1 can be approximated by the linear and the quadratic terms, which are in line with the second-order polynomial fit of Young's modulus extracted by Smith and Ten Cate from the experiments.[32]

Figure 12 shows the gradual recovery of resonant frequency f_r to its maximum limiting value f_0 after the bar was

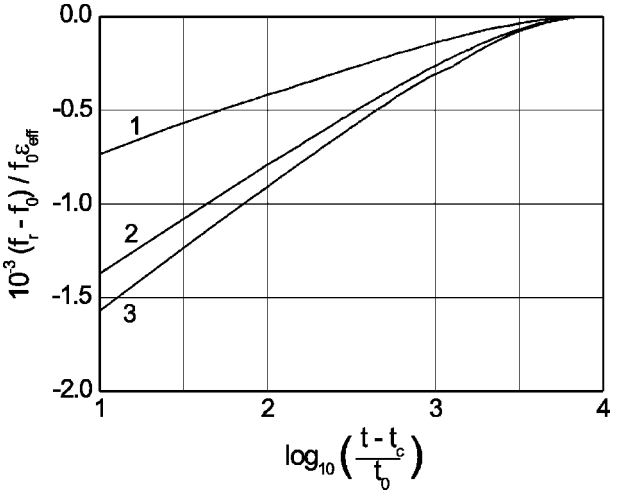

FIG. 12. Time-dependent recovery of peak frequency f_r to its asymptotic value f_0. Curves $j=1,2,3$ correspond to successively higher saturations $s_j=0.05(2j-1)$. The frequency shift f_r-f_0 is normalized by both the asymptotic frequency f_0 and the effective conditioning strain ε_{eff}. Here ε_{eff} is defined as the value of dimensionless response amplitude R/L which had been attained during high-amplitude conditioning tuned to the frequency of resonance.

subjected to high amplitude conditioning and then conditioning was stopped. Conditioning was performed by multiple short-range sweeps over the resonance at the drive level used to obtain the third pair ($j=3$) of curves in Fig. 5. We have plotted three different curves corresponding to three different saturations with all other model parameters used for Fig. 5 retained. The net frequency shift f_r-f_0 consists of two different parts, namely (i) the expected dynamic shift caused by strain nonlinearity at high levels of excitation[31] and (ii) the shift caused by the slow subsystem. However, only the second part can actually be observed during the recovery process because the first vanishes almost instantaneously on switching off the high amplitude drive. Hence, the visible recovery should be governed by the slow kinetics of restoring intergrain cohesive bonds. From Fig. 12 we clearly see the very wide time interval $10t_0<t-t_c<1000t_0$ of logarithmic recovery of resonant frequency f_r, in complete agreement with experimental results[15] and analytical calculations summarized by formulas (34) and (35) from Sec. IV. Here t_c is the moment when conditioning was switched off and $t_0=1$ s is the time scaling constant.

The process of low amplitude probing of recovering resonant frequency to determine f_r as a function of time follows the same procedure either experimentally or theoretically. After the high-amplitude conditioning drive is stopped, a low-amplitude drive remains on to repeatedly sweep the resonance curve and monitor the moving position of resonant frequency f_r. Figure 13 illustrates the set of successive resonance curves corresponding to the time-dependent recovery of resonant frequency given by curve 3 of Fig. 12. At each successive sweep the curves shift upward in frequency and gradually approach an asymptotic curve with the asymptotic resonant frequency f_0 indicated by an arrow. Only a fraction of the successive resonance curves calculated over the time interval $t-t_c>1$ s are clearly distinguishable because separation between neighboring curves progressively diminishes with successive sweeps. The amplitude of the probing drive was taken to be as small as $D=1.14\cdot10^{-9}\ L$.

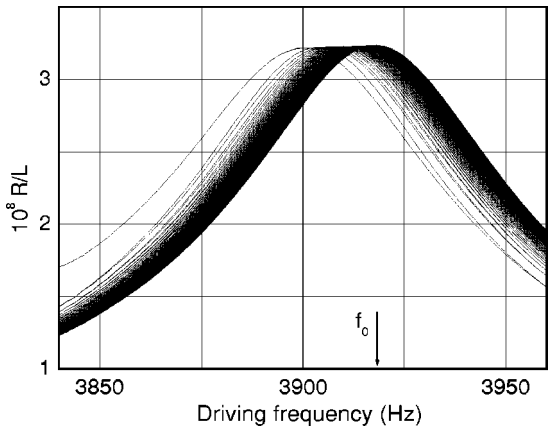

FIG. 13. The set of successive resonance curves obtained by means of back and forth sweeps around the recovering resonance after the high-amplitude conditioning drive was stopped. The arrow indicates the asymptotic resonant frequency. Water saturation, amplitude of probing drive, and absolute value of sweep rate are $s=0.25$, $D=1.14\cdot10^{-9}\ L$, and $|df/dt|=400$ Hz/min.

Another interesting experimental observation is the dramatic suppression of hysteresis with decreasing water saturation.[7] According to our theory this effect can be understood by noting that equilibrium defect concentration in an recovered sample c_0 (13) drops more than three times in magnitude when water saturation decreases from $s=0.25$ to $s=0.05$. Indeed, it is precisely the equilibrium defect concentration (13) that controls variation of elastic modulus (11) through strain-induced variation of nonequilibrium defect concentration c as follows from the kinetic Eq. (7) and formulas (8)–(10). This conclusion has been confirmed by direct computation with saturation $s=0.05$ being the only model parameter changed from the parameters adopted for Fig. 5. The results shown in Fig. 14 contrast in hysteresis with those of Fig. 5. Figure 14 also demonstrates a substan-

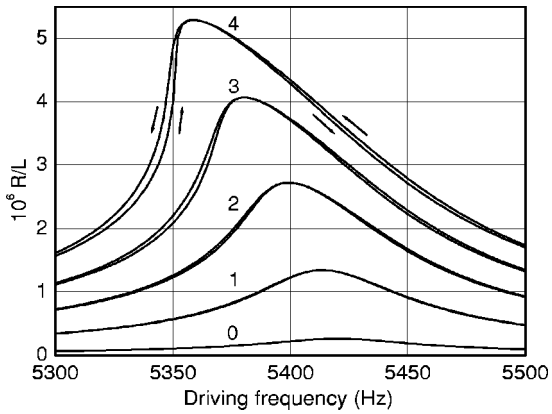

FIG. 14. Conditioned resonance curves $j=0,1,2,3,4$ at successively higher driving amplitudes $D_j=3.8(j+0.2\delta_{j0})10^{-8}\ L$. Arrows on the two highest curves indicate sweep directions. The absolute value of sweep rate is $|df/dt|=400$ Hz/min, and water saturation is $s=0.05$.

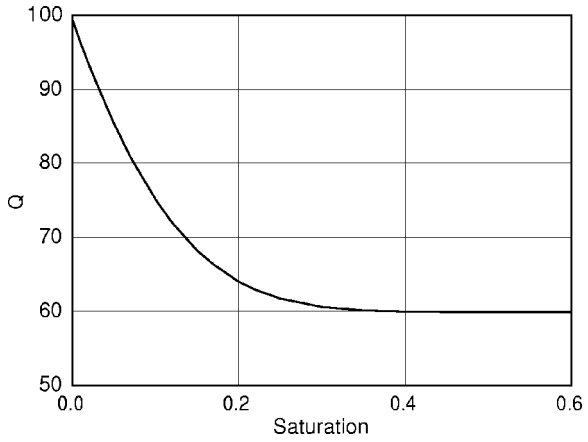

FIG. 15. Quality factor Q as a function of water saturation s. The fixed model parameters were assumed to be the same as for Fig. 5.

tial increase of resonant frequency f_r in comparison with Fig. 5 as a result of the monotonic growth of Young's modulus with decreasing saturation [seen already at $\sigma=0$ from expression (12) combined with formula (13)]. Due to this fact the interval of frequency sweep for producing Fig. 14 was shifted to 5200–5600 Hz.

In addition, we have observed a monotonic decrease in quality factor Q (defined here as resonant frequency f_r divided by the resonance curve width at $\sqrt{2}/2$ of peak height at low-amplitude drive) with increase of water saturation s. This trend is well-documented in numerous experiments.[5–8] In the present theory it derives from the drop of resonant frequency f_r with water saturation s as seen from the low-amplitude analytical estimation at $\sigma=0$ and $\gamma=0$ when the expressions (36), (12), and (13) are combined. Figure 15 illustrates the theoretical dependence of quality factor Q on saturation s with all model parameters except the variable s as given in Fig. 5.

It is worth noticing that the quantitative character of theoretical results depends substantially on the choice of any particular model parameter at fixed other parameters (notice, for example, Figs. 5 and 14 distinguished only by differing water saturations). Nevertheless, there exist at least two possibilities to change several model parameters simultaneously without visible variations in characters of resonance curves. The most evident set of such parameters are three nonlinearity parameters a, r, and cosh η that at low level strains may be replaced by only two of their combinations [see expansion (6)]. Another possibility to obtain a resemblance in resonance curves might be revealed empirically by simultaneous variation of parameters cosh η, v, and U_0 during trial simulations (for example, a decrease of cosh η could be complemented by a concordant increase of v and decrease of U_0, given the sum U_0+U_+ remains fixed). However, analyzing other facets of slow dynamics allows one in principle to rule out such an ambiguity. Still, the main obstacle to the reliable choice of all model parameters is caused by the lack of comprehensive experimental data that ought to be collected on the same specimen (or on the set of equivalent specimens) with the use of all already approbated experimental approaches both dynamic and static.

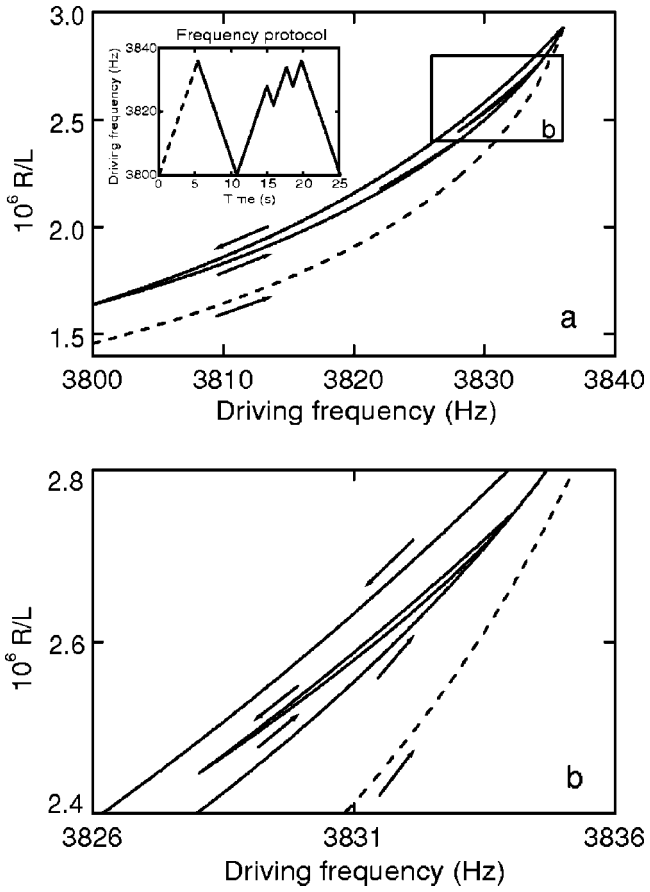

FIG. 16. Manifestation of end-point memory in dynamic response with a multiply-reversed frequency protocol. Model parameters, including the absolute value of sweep rate, coincide with those for the two highest resonance curves in Fig. 5. The range of frequency sweep is on the low-frequency slopes of the two highest resonance curves from Fig. 5. R is the response amplitude taken at the free end of the bar.

There is a further remark about numerical simulations. When discretizing the coordinate variable in the equation for the elastic subsystem the best convergence of the computational procedure is achieved by adjusting the mesh width in such a way that each node of excited standing wave has to be positioned in the closest possible vicinity to some discrete coordinate site.

VI. DYNAMICAL REALIZATION OF END-POINT MEMORY: THEORETICAL PREDICTIONS

Figures 5–7 and 14 demonstrate a dynamical realization of hysteretic phenomena in the case of only two reversing points in the driving frequency protocol. The question arises whether an effect similar to the end-point (discrete) memory that is observed in quasistatic experiments with a multiply-reversed loading-unloading protocol[4,9–11,33] could also be manifested in resonating bar experiments with a multiply-reversed frequency protocol.

We studied this problem theoretically and show the results in Fig. 16, where the model parameters including the absolute value of sweep rate coincide with those of the two highest resonance curves in Fig. 5, while the sweep range is taken within the low-frequency slopes of these curves. End-point memory, defined here as the memory of the previous maximum amplitude of alternating stress, is seen to be pronounced in the form of small loops inside the big loop. The starting and final points of each small loop in Fig. 16 coincide, which is the typical manifestation of end-point memory. A small closed loop can be produced anywhere on the unconditioned (dashed) curve (not shown), but the situation on the conditioned up-going curve looks more complicated. Thus, the closeness of an extremely small loop can be achieved only on the upper part of the conditioned up-going curve. The reason for such behavior is the existence of a threshold stress amplitude (depending on previous history) that must be surmounted in order for the kinetics of the slow subsystem to be switched from defect annihilation at lower amplitudes to defect creation at higher amplitudes. This restriction can be substantially relaxed provided the linear size of the inner loop becomes comparable with that of the big outer loop. Direct calculations (not shown) confirm the earlier statement, and the chance to find the inner loop being closed increases progressively with the growth of its size irrespective of whether the inner loop was produced on an up-going or on a down-going curve of the big outer loop.

VII. CONCLUSION

To summarize, we have performed a systematic analytical and computational simulation of various nonlinear and relaxation phenomena observed experimentally in the nonclassical resonant response of bar-shaped sedimentary rocks when excited by longitudinal standing waves. In particular, we have managed to describe hysteretic behavior of resonance curves, almost linear shift of resonant frequency as a function of driving amplitude, evolution of response amplitude after temporarily stopping a frequency sweep, jumps of resonance curves after temporarily interrupting the external drive (i.e., when sweep and drive were paused simultaneously), suppression of hysteresis at small water saturations, and the decrease of elastic modulus and quality factor with increased saturation. In doing so we have explored both qualitatively and quantitatively the consequences of two coupled subsystems in which mesoscopic defects in a field of internal stress are created and removed at different rates in response to an external drive.

In our treatment the subsystems are as follows: (i) a subsystem of longitudinal displacements and (ii) a subsystem of ruptured intergrain cohesive bonds. This is in apparent contrast with other two-subsystem approaches[34–37] where the second subsystem is associated with auxiliary hysteretic elements. Considering our approach as an alternative to the already known theories[34–37] we would emphasize its principal advantage, namely, the ability to reproduce a remarkably wide class of experimental results by means of a restricted number of physical parameters. The significant points of our model are specified through the coupling between the subsystems on the one hand and the nontrivial (i.e., soft-ratchet) kinetics governing the particular constituent concentration of ruptured bonds on the other. This coupling ensures that the elastic subsystem triggers evolution of the subsystem of ruptured bonds by changing the conditions of their equilibrium, while the subsystem of ruptured bonds affects the elastic subsystem by reducing Young's modulus in proportion to the prevailing concentration of defects. Due to the substantial excess of rupture rate over restoration rate the subsystem of ruptured bonds breaks the symmetry of dynamical response to an alternating external drive in the entire system. This asymmetry produces the majority of nontrivial nonlinear and relaxation effects in sedimentary rocks. Nevertheless, we must bear in mind that the logarithmic recovery of resonant frequency could not be understood without additionally invoking a proper distribution of restoration rates within a considerable but finite interval. Otherwise, recovery kinetics would inevitably shrink into purely exponential decay when the width of the rate distribution tends to zero.

It is necessary to say that despite its success, this model could be further improved to reproduce the preferable generation of odd harmonics as seen in experiments at low excitation levels.[12,38] Following Kadish, Johnson, and Zinszner[38] this modification could be done by introducing nonlinear in place of linear attenuation. Unfortunately, the type of dissipative nonlinearity cannot be strictly established from the experiments,[39] and even the simplest linear form of internal attenuation adopted in the present research might actually originate from several fundamentally different physical mechanisms.[40] Thus, detailed analysis of feasible nonlinear attenuations goes beyond the scope of the present investigation.

Still, even within the framework of the present formalism we have been able to predict an unusual hysteresis with end-point (discrete) memory in an essentially dynamical realization.

As a final remark, the term "slow subsystem" is used as a synonym for the notion "subsystem of ruptured intergrain cohesive bonds." At first sight, this term seems to be incorrect in that the soft-ratchet kinetic Eq. (7) contains two substantially different rates, one of which (the bond rupture rate) may be comparable to or even exceeds the external drive frequency. However, it is precisely the fast rate of bond rupture that ties defect concentrations to strain amplitude when this amplitude is growing. As a result, the effective rate of concentration growth is determined by the slow increase of strain amplitude in an extremely slow frequency sweep. On the other hand, when strain amplitude decreases, then only the slow mechanism of bond restoration is able to work. Thus, the term slow subsystem appears to be reasonable because typical times responsible for the steady evolution of defect concentration turn out to be very large in comparison with the period of alternating strain.

ACKNOWLEDGMENTS

This research was supported by the Science and Technology Center in Ukraine under Grant No. 1747. T.J.S. thanks the Geosciences Research Program, Office of Basic Energy Sciences of the US Department of Energy for sustained assistance. O.O.V. acknowledges support from the National Academy of Sciences of Ukraine (Grant No. 0102U002332).

[1] R. E. Collins, *Flow of Fluids through Porous Materials* (Reinhold, New York, 1961).
[2] F. A. L. Dullien, *Porous Media. Fluid Transport and Pore Structure* (Academic Press, New York, 1979).
[3] J.-F. Thovert, F. Yuosefian, P. Spanne, C. G. Jacquin, and P. M. Adler, Phys. Rev. E **63**, 061307 (2001).
[4] R. A. Guyer and P. A. Johnson, Phys. Today **52**, 30 (1999).
[5] V. A. Clark, B. R. Tittmann, and T. W. Spencer, J. Geophys. Res. B **85**, 5190 (1980).
[6] B. Zinszner, P. A. Johnson, and P. N. J. Rasolofosaon, J. Geophys. Res., [Solid Earth] **102**, 8105 (1997).
[7] K. E.-A. Van Den Abeele, J. Carmeliet, P. A. Johnson, and B. Zinszner, J. Geophys. Res., [Solid Earth] **107**, 2121 (2002).
[8] B. R. Tittmann, V. A. Clark, J. M. Richardson, and T. W. Spencer, J. Geophys. Res. B **85**, 5199 (1980).
[9] N. G. W. Cook and K. Hodgson, J. Geophys. Res. **70**, 2883 (1965).
[10] R. B. Gordon and L. A. Davis, J. Geophys. Res. **73**, 3917 (1968).
[11] P. A. Johnson and P. N. J. Rasolofosaon, Nonlinear Processes Geophys. **3**, 77 (1996).
[12] P. A. Johnson, B. Zinszner, and P. N. J. Rasolofosaon, J. Geophys. Res., [Solid Earth] **101**, 11553 (1996).
[13] J. A. Ten Cate and T. J. Shankland, Geophys. Res. Lett. **23**, 3019 (1996).
[14] R. A. Guyer, J. Ten Cate, and P. Johnson, Phys. Rev. Lett. **82**, 3280 (1999).
[15] J. A. Ten Cate, E. Smith, and R. A. Guyer, Phys. Rev. Lett. **85**, 1020 (2000).
[16] J. A. Ten Cate and T. J. Shankland, in *Proceedings of the 16th International Congress on Acoustics and 135th Meeting of the Acoustical Society of America*, edited by P. A. Kuhl and L. A. Crum (American Institute of Physics, New York, 1998), Vol. 3, p. 1565.
[17] R. A. Guyer, K. R. McCall, and K. Van Den Abeele, Geophys. Res. Lett. **25**, 1585 (1998).
[18] O. O. Vakhnenko, V. O. Vakhnenko, T. J. Shankland, and J. A. Ten Cate, Phys. Rev. E **70**, 015602(R) (2004).
[19] N. V. Vasylenko, *Teoriya Kolebaniy* (Vyshcha Shkola, Kyïv, 1992).
[20] G. G. Stokes, Cambridge Transactions **8**, 287 (1845).
[21] A. M. Kosevich, *Osnovy Mekhaniki Kristallicheskoy Reshetki* (Nauka, Moscow, 1972).
[22] A. M. Kosevich, *Fizicheskaya Mekhanika Real'nykh Kristallov* (Naukova Dumka, Kyïv, 1981).
[23] A. S. Nowick and B. S. Berry, *Anelastic Relaxation in Crystalline Solids* (Academic Press, New York, 1972).
[24] A. Kaselow and S. A. Shapiro, J. Geophys. Eng. **1**, 1 (2004).
[25] W. Sutherland, Philos. Mag. **32**, 31 (1891).
[26] C. Zener, *Elasticity and Anelasticity of Metals* (The University of Chicago Press, Chicago, 1948).
[27] J. A. Ten Cate, J. Duran, and T. J. Shankland, in *Proceedings of the 16th International Symposium on Nonlinear Acoustics*, edited by O. V. Rudenko and O. A. Sapozhnikov (MSU, Moscow, 2002), Vol. 2, p. 767.
[28] Yu. N. Rabotnov, *Elementy Nasledstvennoy Mekhaniki Tverdykh Tel* (Nauka, Moscow, 1977).
[29] G. A. Korn and T. M. Korn, *Mathematical Handbook for Scientists and Engineers. Definitions, Theorems and Formulas for Reference and Review* (McGraw-Hill, New York, 1961).
[30] L. Bocquet, E. Charlaix, S. Ciliberto, and J. Crassous, Nature (London) **396**, 735 (1998).
[31] N. N. Bogolyubov and Yu. A. Mytropol'skiy, *Asymptoticheskiye Metody v Teorii Nelineynykh Kolebaniy* (Nauka, Moscow, 1974).
[32] E. Smith and J. A. Ten Cate, Geophys. Res. Lett. **27**, 1985 (2000).
[33] R. A. Guyer, K. R. McCall, G. N. Boitnott, L. B. Hilbert, Jr., and T. J. Plona, J. Geophys. Res., [Solid Earth] **102**, 5281 (1997).
[34] B. Capogrosso-Sansone and R. A. Guyer, Phys. Rev. B **66**, 224101 (2002).
[35] M. Scalerandi, P. P. Delsanto, and P. A. Johnson, J. Phys. D **36**, 288 (2003).
[36] P. P. Delsanto and M. Scalerandi, Phys. Rev. B **68**, 064107 (2003).
[37] M. Nobili and M. Scalerandi, Phys. Rev. B **69**, 104105 (2004).
[38] A. Kadish, P. A. Johnson, and B. Zinszner, J. Geophys. Res., [Solid Earth] **101**, 25139 (1996).
[39] Ya. G. Panovko, *Vvedeniye v Teoriyu Mekhanicheskikh Kolebaniy* (Nauka, Moscow, 1991).
[40] Yu. N. Rabotnov, *Mekhanika Deformiruyemogo Tverdogo Tela* (Nauka, Moscow, 1979).